Absence of topological β-antimonene and growth of α-antimonene on noble metal Ag(111) and Cu(111) surfaces

Ping Zhang [1,2] Chen Ma,[1,2] Shaoxiang Sheng [1,2] Huiru Liu,[1,2] Jisong Gao,[1,2] Zijia Liu,[1,2] Peng Cheng,[1,2] Baojie Feng [1,2,3,*] Lan Chen,[1,2,4] and Kehui Wu[1,2,3,4,†]

[1]*Institute of Physics, Chinese Academy of Sciences, Beijing 100190, China*
[2]*School of Physical Sciences, University of Chinese Academy of Sciences, Beijing, 100190, China*
[3]*Interdisciplinary Institute of Light-Element Quantum Materials and Research Center for Light-Element Advanced Materials,*
Peking University, Beijing, 100871, China
[4]*Songshan Lake Materials Laboratory, Dongguan, Guangdong, 523808, China*

Antimonene is a promising two-dimensional material predicted to host intriguing properties. Recent works have claimed the successful preparation of β-antimonene on noble metal surfaces, including Ag(111) and Cu(111). However, as scanning tunneling microscopy gives only the topographic information, the possibility of surface alloying for the claimed β-antimonene remains elusive. In this work, by scanning tunneling spectroscopy and *in situ* Raman spectroscopy measurements, we provide compelling evidence that the "β-antimonenes" on Ag(111) and Cu(111) reported in previous studies are both surface alloys, namely, Ag_2Sb and Cu_2Sb. Thus, β-antimonene does not exist on these substrates. Instead, we find that α-antimonene can be grown on both alloy surfaces, with different substrate-induced strain modulation effects. Our work not only clarifies the growth dynamics of Sb on Ag(111) and Cu(111) but also provides two model systems to realize α-antimonene with tunable strains.

I. INTRODUCTION

Antimonene is the two-dimensional (2D) polymorph of group V element antimony. As an emerging 2D material, it is predicted to host interesting properties such as ferroelectricity [1], thermoelectricity [2,3], high carrier mobility [2,4], and high optical refractive index in the ultraviolet region [5]. To date, two stable phases, α and β [6], have been synthesized [7]. The α-antimonene, which has a puckered honeycomb structure, is expected to host intriguing electronic and optoelectronic properties because of its similarity with black phosphorus (BP). Because of the lack of bulk counterparts, α-antimonene can only be synthesized by epitaxial growth. To date, α-antimonene has been successfully synthesized on several substrates such as SnSe, WTe_2, $MoTe_2$, and Bi_2Se_3 [8–11].

On the other hand, β-antimonene is the monolayer of bulk antimony and can be directly isolated by mechanical exfoliation. In addition, β-antimonene has also been predicted and claimed to be synthesized by molecular beam epitaxy (MBE) on Ag(111) and Cu(111) [12–17]. Different structure models have been proposed, including β-antimonene on unreconstructed or alloyed surfaces. Since both β-antimonene and Ag_2Sb/Cu_2Sb alloys exhibit similar sixfold symmetric structures, it is difficult to distinguish them only by STM measurements. As a powerful technique to study the vibrational

properties of materials, Raman spectroscopy can provide fingerprint features for 2D materials. However, conventional ambient Raman spectroscopy is not applicable because of the easy degradation of antimonene in air [18]. Therefore, to clarify the exact structure and composition of these surface structures, combined STM and *in situ* Raman spectroscopy measurements are highly desirable.

In this paper, we clarify the growth dynamics of Sb on Ag(111) and Cu(111) substrates by a combined scanning tunneling microscopy/spectroscopy (STM/STS) and *in situ* Raman spectroscopy study. Even at room temperature (RT), Sb will seriously alloy with Ag and Cu, forming Cu_2Sb and Ag_2Sb alloy islands. Notably, large-area and atomically flat Cu_2Sb and Ag_2Sb alloy can form on the surfaces after annealing at appropriate temperatures, which were assigned as "β-antimonene" in previous studies [12–15]. On the other hand, further deposition of Sb atoms on alloy surfaces can result in the formation of α-antimonene, as evidenced by its STM topography and Raman fingerprint. The as-prepared α-antimonene exhibits significant strain on the two substrates, up to 5.9% (expansion) and –2.7% (compression), respectively. Our study clarifies the growth dynamics of Sb on noble metal Cu and Ag surfaces and provides an effective method to manipulate the properties of α-antimonene by substrate-induced strain effects.

II. METHODS

The experiments were performed in an ultrahigh vacuum (UHV) system consisting of a preparation chamber

---
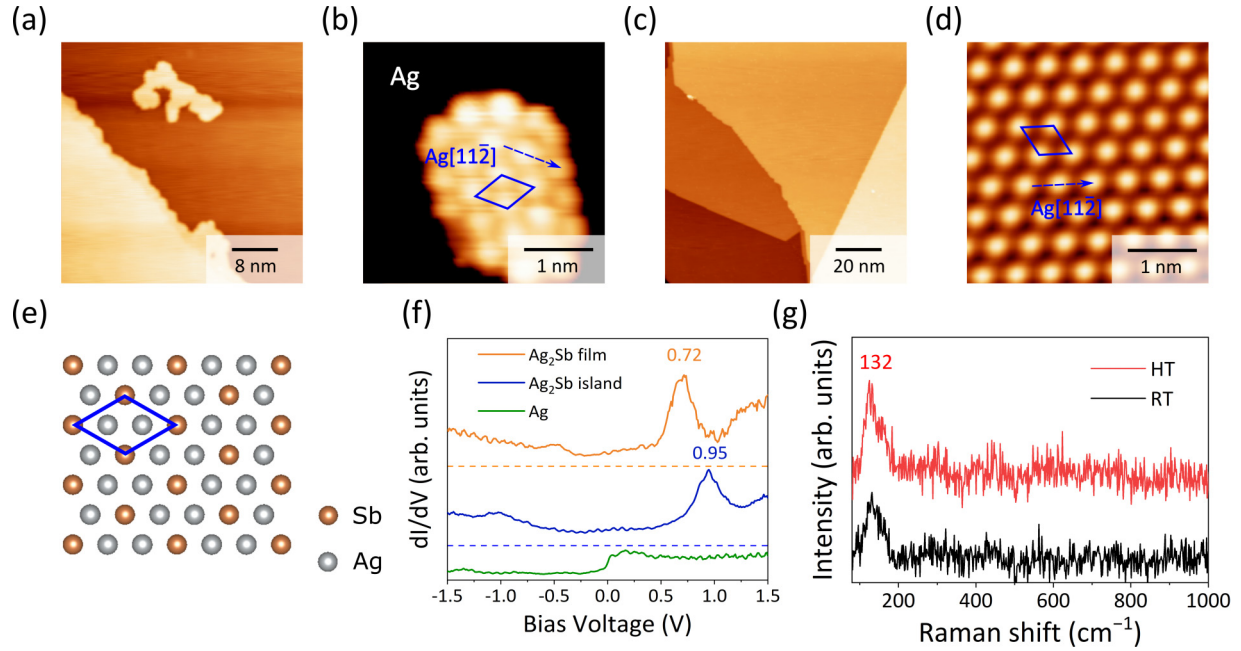
*bjfeng@iphy.ac.cn
†khwu@iphy.ac.cn

FIG. 1. (a) STM image (−0.5 V, −100 pA) of a typical alloy island after less than 1 ML of Sb was deposited on Ag(111) at RT. (b) High-resolution STM image (−0.5 V, −100 pA) of an alloy island. (c) STM image (−0.5 V, −100 pA) of the 1 ML sample after annealing at 360 K for 1 h. (d) High-resolution STM image (−1 V, −50 pA) of (c). (e) Structure model of Ag_2Sb surface alloy. (f) STS spectra taken on alloy islands (−1.5 V, −100 pA), alloy film (−1.5 V, −100 pA), and pristine Ag(111) (−1.5 V, −40 pA), respectively. (g) *In situ* Raman spectra (532 nm, 10 mW, each spectrum at 10 min) of the Sb/Ag(111) obtained at RT and HT, respectively.

and an STM chamber. The base pressure of the system is greater than 1×10^{-10} Torr. Single-crystal Ag(111) and Cu(111) surfaces were cleaned by standard Ar^+ ion sputtering and annealing cycles. High-purity Sb was evaporated from a Knudsen cell. The minimum and maximum temperatures to prepare α-antimonene on Ag_2Sb (Cu_2Sb) are 340 K (300 K) and 370 K (330 K), respectively. STM and STS measurements were performed at 5 K with a chemically etched W tip. For STS measurements, a lock-in amplifier was used with a sinusoidal voltage modulation (20 mV, 659 Hz). Monolayer Ag_2Sb (Cu_2Sb) refers to an Sb concentration of $4.6 \times 10^{14} (5.9 \times 10^{14})$ atoms/cm^2, which corresponds to one-third of the surface atomic density of the Ag(111) [Cu(111)] surface. Monolayer α-antimonene on Ag_2Sb (Cu_2Sb) refers to an Sb concentration of $1.84 \times 10^{15} (1.92 \times 10^{15})$ atoms/cm^2.

The Raman spectra were measured in the STM chamber, with a side illumination and backscattering collection configuration. A 532 nm/632.8 nm laser was induced through the UHV window and focused on the sample surface using an adjustable aspheric lens inside the UHV chamber. The scattered far-field Raman signal was collected outside the window and analyzed by an imaging spectrograph (Princeton Instruments) with a liquid-nitrogen-cooled charge coupled device (CCD). We confirmed that all the samples remained unchanged after laser illumination by STM topography taken after Raman measurements. To exclude the influence of substrates, we detected their Raman signal at first and could not observe any characteristic peak, as shown in Fig. S1 in the Supplemental Material [19]. All the structure models were plotted by VESTA [20].

III. RESULTS AND DISCUSSIONS

A. Sb on Ag(111)

We first investigate the growth of Sb on Ag(111). When less than one monolayer (ML) Sb was deposited on Ag(111) substrate at RT, we observed the formation of monolayer (ML) islands with smooth surfaces but irregular shapes, as shown in Fig. 1(a). A high-resolution STM image on the surface of these islands [Fig. 1(b)] revealed a hexagonal structure. The lattice constant is approximately 0.502 nm, which matches $\sqrt{3}$ times that of Ag (111). The close-packing direction of the lattice, as marked by the blue line, is along the [11$\bar{2}$] direction of the Ag substrate, indicating a $\sqrt{3} \times \sqrt{3}R30°$ superstructure. With increasing Sb coverage, the total area of these islands increases. Note that the second-layer islands will start to grow before the completion of the first layer (see Fig. S2 in the Supplemental Material [19]).

When the sample with Sb coverage of about 1 ML was annealed at 370 K for 1 h, a highly ordered and atomically smooth surface formed, as shown in Fig. 1(c). The high-resolution STM image in Fig. 1(d) shows a well-ordered $\sqrt{3} \times \sqrt{3}R30°$ structure. It should be noted that both the RT and high-temperature (HT) superstructures have been reported in previous studies. However, either the RT and HT superstructures were previously assigned to be β-antimonene [14,15]. It was argued that β-antimonene can form as Sb-Ag alloying was suppressed by either low-temperature annealing or preformed Ag-Sb alloy surfaces. In our case, it is obvious that the initial islands contain Ag-Sb alloy, as the islands and the substrate surface exhibit an identical $\sqrt{3} \times \sqrt{3}R30°$ structure. In addition, one can see single dark sites and protrusions
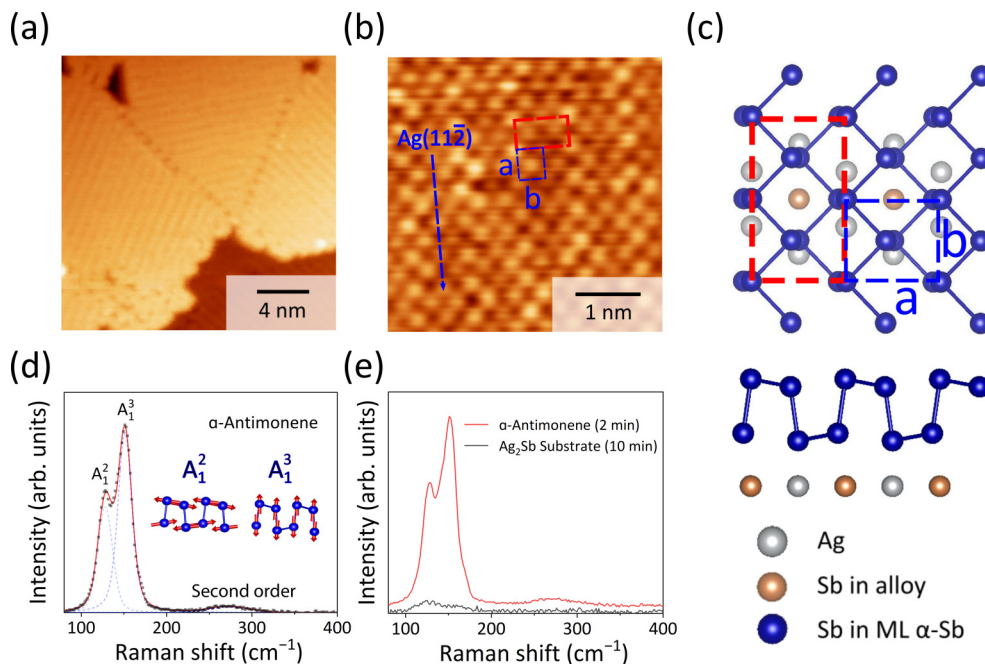
FIG. 2. (a) STM image (-0.5 V, -100 pA) of 0.8 ML α-antimonene grown on $Ag_2Sb/Ag(111)$. (b) High-resolution STM image (-0.35 V, -150 pA) of α-antimonene. (c) Structure model of α-antimonene on Ag_2Sb. (d) *In situ* Raman spectrum (532 nm, 10 mW, 2 min) of α-antimonene. (e) *In situ* Raman spectra (532 nm, 10 mW) of 0.8 ML α-antimonene and the Ag_2Sb substrate, respectively.

on the substrate surface, indicating that the substrate Ag atoms were replaced by Sb atoms, as shown in Fig. S3 [19]. The most likely structure model of the $\sqrt{3} \times \sqrt{3} R 30°$ surface is monolayer Ag_2Sb on Ag(111) according to previous studies [21,22,30], as illustrated in Fig. 1(e).

The STS spectra shown in Fig. 1(f) indicate that the $\sqrt{3} \times \sqrt{3} R 30°$ structures formed at RT and HT exhibit similar features. We observed a characteristic peak at 0.95 and 0.72 eV for RT and HT structures, respectively. The similar STS features indicate that they are the same structure. The slight shift of the characteristic peak can be accounted for by the better order of the surface in the latter case or the quantum confinement by the periphery of the islands in the former case. Moreover, *in situ* Raman measurements further support our conclusion. As shown in Fig. 1(g), the Raman signals of the RT and HT samples exhibit a similar peak near 132 cm^{-1}, which is quite different from the Raman spectrum of β-antimonene in previous reports [23–25] either for bulk or monolayers, which exhibit two apparent peaks near 120 and 150 cm^{-1}. Thus, we conclude that the $\sqrt{3} \times \sqrt{3} R 30°$ structures formed at RT and HT are both Ag_2Sb alloys.

The formation of Ag_2Sb surface alloy is not surprising, according to the binary alloy phase diagram between Ag and Sb. Similar surface alloys have been reported in many binary metal systems [26,27]. However, when more Sb atoms were deposited on the Ag_2Sb surface, the increased chemical potential of Sb and limited diffusion length of Sb into the bulk Ag may result in the growth of pure Sb layers, namely, antimonene. We have investigated this possibility by depositing Sb on the HT Ag_2Sb alloy surface at RT. The as-grown surface is flat but slightly disordered. After annealing at 360 K, a well-ordered phase is formed. This phase is characterized by long-range parallel stripes with a distance of $\sim$0.862 nm, as

shown in the STM image [Fig. 2(a)]. The "stripes" are along the close-packed direction of the Ag_2Sb substrate, as indicated by the blue line. A zoomed-in STM image is displayed in Fig. 2(b), which shows a rectangular lattice with lattice constants of 0.502 and 0.431 nm. We note that this phase is quite similar to freestanding α-antimonene ($a = 0.474$ nm, $b = 0.436$ nm) [6], but has a 5.9% lattice expansion in the armchair direction and 1.1% compression in the zigzag direction. In addition, we observed a 1×2 superstructure, as indicated by the red rectangle in Fig. 2(b). The structure model of the α-antimonene on Ag_2Sb is shown in Fig. 2(c). As the Ag and Sb atoms have different interactions with antimonene, the Sb atom in antimonene directly above an Sb atom looks brighter in STM images, resulting in the 1×2 moiré pattern.

Next, we performed *in situ* Raman measurements to confirm the structure of this phase, as shown in Figs. 2(d) and 2(e). The Raman spectrum shows three characteristic peaks at 128, 152, and 273 cm^{-1}, respectively. The first two peaks accord well with the A_1^2 and A_1^3 modes of α-antimonene [6,8], and the third peak can be associated with the second-order Raman scattering [28]. Notably, the relative Raman intensity of α-antimonene is much stronger than that of the Ag_2Sb alloy, as shown in Fig. 2(e). With the same Raman measurement configuration, the Raman intensity of α-antimonene collected in 2 min is 14 times higher than that of the Ag_2Sb alloy collected in 10 min. The weak Raman intensity of the Ag_2Sb alloy might originate from the screen of the incident light by the Ag(111) substrate; the screening effect becomes less pronounced for antimonene on Ag_2Sb. The apparent difference between 2D materials and surface alloy has also been reported in germanene and Ge-Au alloy [29]. Therefore, our combined STM and Raman measurements unambiguously pin down this structure as α-antimonene.
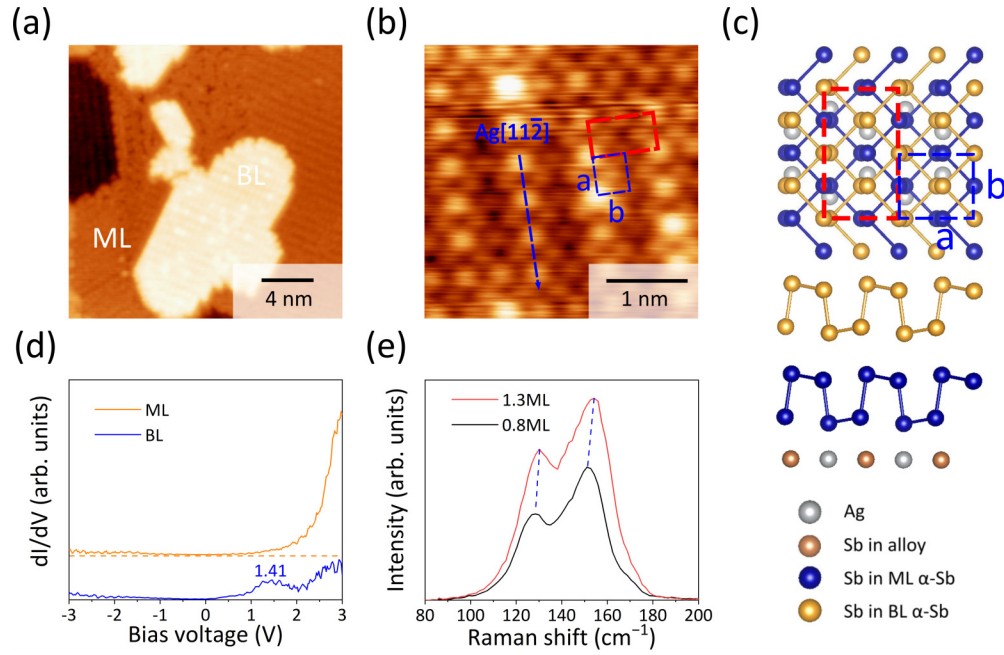
FIG. 3. (a) STM image (-0.1 V, -100 pA) of 1.3 ML α-antimonene grown on Ag_2Sb/Ag(111). (b) High-resolution STM image (-0.95 V, -100 pA) of bilayer α-antimonene. (c) Structure model of bilayer α-antimonene on Ag_2Sb. (d) STS spectra (-3 V, -100 pA) of monolayer and bilayer α-antimonene. (e) *In situ* Raman spectra (532 nm, 10 mW) of α-antimonene with different coverage.

After the entire surface is covered by monolayer α-antimonene, further increasing the Sb coverage will result in the growth of bilayer (BL) α-antimonene [Fig. 3(a)]. As the high-resolution STM image [Fig. 3(b)] shows, the bilayer α-antimonene looks identical to the 1 ML α-antimonene. The most likely model of bilayer α-antimonene is shown in Fig. 3(c).

We then performed STS and *in situ* Raman measurements on α-antimonene with different thicknesses. As shown in Fig. 3(d), the STS spectra of both monolayer and bilayer α-antimonene show a metallic feature, similar to that of Ag_2Sb. However, the characteristic peak of Ag_2Sb at 0.72 eV is absent on antimonene. Notably, monolayer α-antimonene has increasing density of states above 1.5 eV while bilayer α-antimonene has an obvious peak at 1.41 eV. The thickness dependence of the electronic states of α-antimonene is consistent with previous predictions and experimental results [6,9]. The Raman spectra of monolayer and bilayer α-antimonene are shown in Fig. 3(e). Compared with monolayer samples, the two characteristic Raman peaks of bilayer samples exhibit a slight blueshift (2 and 3 cm^{-1}), which can be explained by the strain relaxation in thicker films.

When the α-antimonene sample was annealed at a relatively high temperature ($\sim$400 K) for 1 h, the whole surface will recover to the Ag_2Sb alloy surface (Fig. S4(a) [19]). Meanwhile, the Raman signal also recovered to that of the Ag_2Sb alloy (Fig. S4(b) [19]). This phenomenon clarifies that previously claimed "β-antimonene" on Ag-Sb alloy obtained at high coverage and substrate temperature [15] is also Ag_2Sb alloy. Notably, Sun *et al.* reported that a distorted antimonene can form on Ag_2Sb with fine tuning of the growth parameters [16], but such structure was not observed in our systematic experiments.

B. Sb on Cu(111)

The growth of Sb on Cu(111) has been reported in several works [7,30–32], where β-antimonene has also been claimed to form [12,13]. Here, we grew Sb on Cu(111) following the same procedure as we did on Ag(111). When less than 1 ML of Sb atoms were deposited on Cu(111) at RT, small islands with irregular shapes are observed, as shown in Fig. 4(a). As shown in the high-resolution STM image in Fig. 4(b), the surface of these islands has a close-packed structure with a lattice constant of 0.447 nm, matching to $\sqrt{3}$ times that of the Cu(111) substrate. In addition, the lattice has a 30° rotation with respect to the $[1\bar{1}0]$ direction of Cu(111), which indicates the formation of $\sqrt{3} \times \sqrt{3}R30^\circ$ superstructure.

Similar to Ag_2Sb/Ag(111), these islands can be interpreted as a Cu_2Sb surface alloy on Cu(111) [30–32], a stable alloy in the phase diagram of Sb and Cu [Fig. 4(e)]. Besides the alloy islands, the substrate surfaces are also partially converted to an identical $\sqrt{3} \times \sqrt{3}R30^\circ$ superstructure, as shown in Fig. 4(b). Moreover, one can see single dark sites and protrusions on the substrate surface, indicating the presence of interchanged individual Cu and Sb atoms. Therefore, we conclude that a Cu_2Sb surface alloy is formed.

Annealing the sample with Sb coverage of more than 1 ML at 550 K can result in the formation of a highly ordered and atomically smooth surface [Fig. 4(c)]. This surface has a similar $\sqrt{3} \times \sqrt{3}R30^\circ$ superstructure as the Cu_2Sb alloy islands obtained at RT, as shown in the high-resolution STM image in Fig. 4(d). Previously, this highly ordered structure was assigned to β-antimonene [13]. However, our STS and *in situ* Raman measurements proved that this phase is also a Cu_2Sb alloy. As Fig. 4(f) shows, the STS spectrum taken on HT samples is similar to that taken on RT samples. We observed a peak at $\sim$1.66 eV, similar to the case of Ag_2Sb.
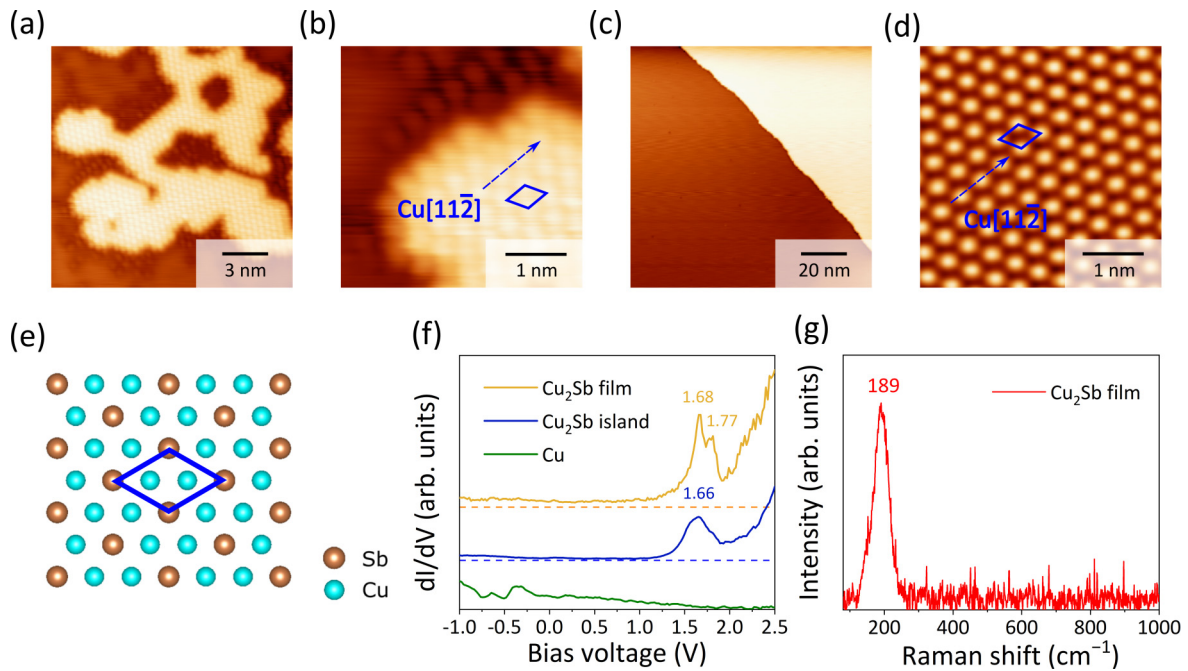
FIG. 4. (a) STM image (-0.5 V, -100 pA) of a typical alloy island after less than 1 ML of Sb was deposited on Cu(111) at RT. (b) High-resolution STM image (-0.5 V, -100 pA) of an alloy island in (a). (c) STM image (-1.5 V, -100 pA) of the 1 ML sample after annealing at 550 K. (d) High-resolution STM image (-0.4 V, -100 pA) of (c). (e) Structure model of Cu_2Sb surface alloy. (f) STS spectra taken on alloy island (-2.5 V, -200 pA), alloy film (-2.5 V, -250 pA), and pristine Cu(111) (-1 V, -100 pA), respectively. (g) *In situ* Raman spectrum (632.8 nm, 16 mW, 8 h) of (c).

More importantly, the Raman spectrum of the HT sample shows only a weak Raman peak at 189 cm^{-1} [Fig. 4(g)], which is different from the expected Raman character of β-antimonene [23–25]. Therefore, we can conclude that both phases are Cu_2Sb alloys rather than β-antimonene, similar to the case of Ag_2Sb/Ag(111).

Similarly, large-area flat islands formed when Sb atoms were deposited on Cu_2Sb at RT with subsequent annealing at 320 K, as shown in Fig. 5(a). We examined whether similar behavior occurs in the case of Sb/Cu(111). Similarly, large-area flat islands formed when Sb atoms were deposited on Cu_2Sb at RT with subsequent annealing at 320 K, as shown in Fig. 5(a). A high-resolution STM image [Fig. 5(b)] indicates that these islands have a rectangular structure with lattice constants of 0.461 and 0.449 nm. This structure corresponds to α-antimonene with 2.7% compression strain in the armchair direction and 3.0% tensile strain in the zigzag direction [Fig. 5(c)].

To further confirm our assignment of the rectangular structure to α-antimonene, we performed *in situ* Raman measurements. As shown in Fig. 5(d), we observed three prominent peaks, similar to the case of α-antimonene on Ag_2Sb. The two peaks at 142 and 159 cm^{-1} are associated with the A_1^2 and A_1^3 modes of α-antimonene but have a slight blueshift compared with α-antimonene on Ag_2Sb. Meanwhile, the second-order Raman scattering peak is shifted from 273 to 284 cm^{-1}. The blueshift of the Raman peaks can be explained by the different strain effects induced by the two substrates. In addition, as Fig. 5(e) shows, the relative Raman intensity of α-antimonene on Cu_2Sb collected in 30 min is about 7 times stronger than that of the substrate collected in

2 h, which is again similar to the case of α-antimonene on Ag_2Sb. Thus, our Raman measurements not only revealed the intrinsic difference between antimonene and Cu_2Sb alloy but also clarified the strain effects on the vibrational modes of α-antimonene.

Finally, when the sample was annealed at 550 K for 1 h, α-antimonene completely disappeared, accompanied by a surface recovery to Cu_2Sb alloy, as evidenced by STM and Raman measurements (Figs. S5(a) and S5(b) [19]). Therefore, the previously claimed "β-antimonene" formed on Cu_2Sb alloy [12] is also Cu_2Sb alloy.

IV. CONCLUSION

In summary, we performed combined STM/STS and *in situ* Raman measurements to investigate the growth dynamics of Sb on Ag(111) and Cu(111). Our results unambiguously proved that the previously reported "β-antimonene" on these substrates is antimonial alloy. In addition, we realized α-antimonene on both surfaces. The as-prepared α-antimonene has a strong lattice strain induced by the substrates, which results in a dramatic change in the electronic and vibrational properties. Our work not only clarified the growth behavior Sb on Ag(111) and Cu(111) but also established *in situ* STM and Raman spectroscopy as a powerful tool to study the growth dynamics of 2D materials.
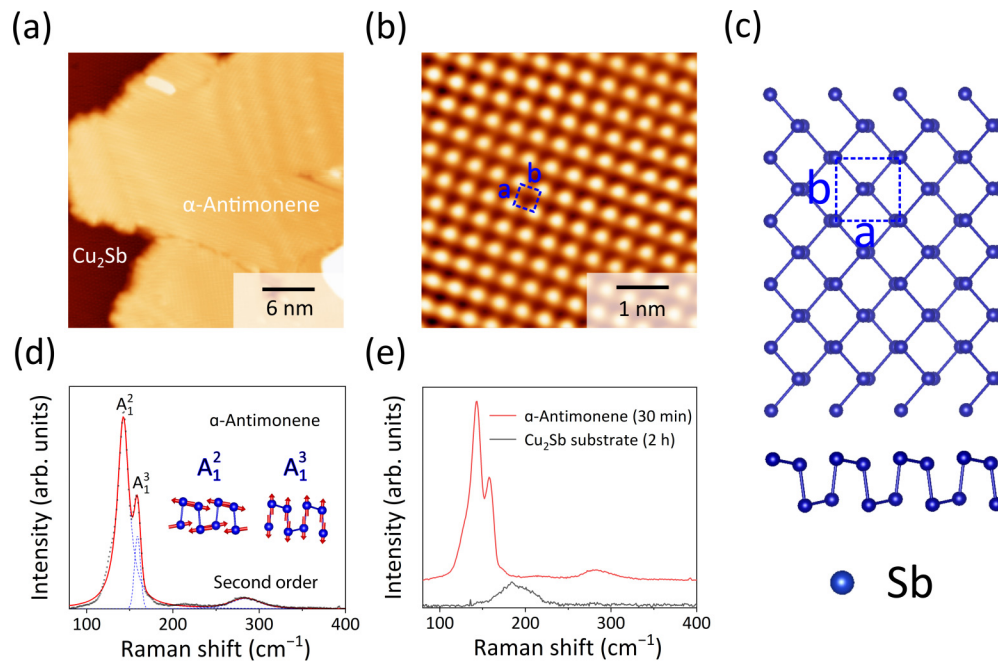
FIG. 5. (a) STM image (-0.5 V, -100 pA) of 0.5 ML α-antimonene grown on Cu$_2$Sb/Cu(111). (b) High-resolution STM image (-0.5 V, -100 pA) of α-antimonene. (c) The model of strained α-antimonene. (d) *In situ* Raman spectrum (632.8 nm, 16 mW, 2 min) of α-antimonene. (e) *In situ* Raman spectra (632.8 nm, 16 mW) 0.5 ML α-antimonene and the Cu$_2$Sb substrate, respectively.

[1] C. Xiao, F. Wang, S. A. Yang, Y. Lu, Y. Feng, and S. Zhang, Adv. Funct. Mater. **28**, 1707383 (2018).

[2] Y. Wu, K. Xu, C. Ma, Y. Chen, Z. Lu, H. Zhang, Z. Fang, and R. Zhang, Nano Energy **63**, 103870 (2019).

[3] K.-X. Chen, S.-S. Lyu, X.-M. Wang, Y.-X. Fu, Y. Heng, and D.-C. Mo, J. Phys. Chem. C **121**, 13035 (2017).

[4] Y. Wang, P. Huang, M. Ye, R. Quhe, Y. Pan, H. Zhang, H. Zhong, J. Shi, and J. Lu, Chem. Mater. **29**, 2191 (2017).

[5] D. Singh, S. K. Gupta, Y. Sonvane, and I. Lukačević, J. Mater. Chem. C **4**, 6386 (2016).

[6] G. Wang, R. Pandey, and S. P. Karna, ACS Appl. Mater. Interfaces **7**, 11490 (2015).

[7] C.-L. Xue and S.-C. Li, Jpn. J. Appl. Phys. **60**, SE0805 (2021).

[8] Z. Q. Shi, H. Li, Q. Q. Yuan, Y. H. Song, Y. Y. Lv, W. Shi, Z. Y. Jia, L. Gao, Y. B. Chen, W. Zhu *et al.*, Adv. Mater. **31**, 1806130 (2019).

[9] Z. Q. Shi, H. Li, C. L. Xue, Q. Q. Yuan, Y. Y. Lv, Y. J. Xu, Z. Y. Jia, L. Gao, Y. Chen, W. Zhu *et al.*, Nano Lett. **20**, 8408 (2020).

[10] C. Hogan, K. Holtgrewe, F. Ronci, S. Colonna, S. Sanna, P. Moras, P. M. Sheverdyaeva, S. Mahatha, M. Papagno, Z. S. Aliev *et al.*, ACS Nano **13**, 10481 (2019).

[11] Z. Q. Shi, H. Li, Q. Q. Yuan, C. L. Xue, Y. J. Xu, Y. Y. Lv, Z. Y. Jia, Y. Chen, W. Zhu, and S. C. Li, ACS Nano **14**, 16755 (2020).

[12] T. Niu, W. Zhou, D. Zhou, X. Hu, S. Zhang, K. Zhang, M. Zhou, H. Fuchs, and H. Zeng, Adv. Mater. **31**, 1902606 (2019).

[13] S. Y. Zhu, Y. Shao, E. Wang, L. Cao, X. Y. Li, Z. L. Liu, C. Liu, L. W. Liu, J. O. Wang, K. Ibrahim *et al.*, Nano Lett. **19**, 6323 (2019).

[14] Y. Shao, Z. L. Liu, C. Cheng, X. Wu, H. Liu, C. Liu, J. O. Wang, S. Y. Zhu, Y. Q. Wang, D. X. Shi *et al.*, Nano Lett. **18**, 2133 (2018).

[15] Y.-H. Mao, L.-F. Zhang, H.-L. Wang, H. Shan, X.-F. Zhai, Z.-P. Hu, A.-D. Zhao, and B. Wang, Front. Phys. **13**, 138106 (2018).

[16] S. Sun, T. Yang, Y. Z. Luo, J. Gou, Y. Huang, C. Gu, Z. Ma, X. Lian, S. Duan, A. T. S. Wee *et al.*, J. Phys. Chem. Lett. **11**, 8976 (2020).

[17] K. Liu, K. Bai, J. Wang, J. Song, and Y. Liu, Front. Phys. **10**, 856526 (2022).

[18] X. Sun, Z. Lu, Y. Xiang, Y. Wang, J. Shi, G. C. Wang, M. A. Washington, and T. M. Lu, ACS Nano **12**, 6100 (2018).

[19] See Supplemental Material at http://link.aps.org/supplemental/10.1103/PhysRevMaterials.6.074002 for additional Raman and STM measurement results.

[20] K. Momma and F. Izumi, J. Appl. Crystallogr. **41**, 653 (2008).

[21] T. C. Q. Noakes, D. A. Hutt, C. F. McConville, and D. P. Woodruff, Surf. Sci. **372**, 117 (1997).

[22] S. Oppo, V. V. Fiorentini, and M. Scheffler, Phys. Rev. Lett. **71**, 2437 (1993).

[23] M. Fortin-Deschenes, R. M. Jacobberger, C. A. Deslauriers, O. Waller, E. Bouthillier, M. S. Arnold, and O. Moutanabbir, Adv. Mater. **31**, 1900569 (2019).

[24] X. Wang, K. Kunc, I. Loa, U. Schwarz, and K. Syassen, Phys. Rev. B **74**, 134305 (2006).

[25] W. Lin, Y. Lian, G. Zeng, Y. Chen, Z. Wen, and H. Yang, Nano Res. **11**, 5968 (2018).

[26] K. H. L. Zhang, I. M. McLeod, Y. H. Lu, V. R. Dhanak, A. Matilainen, M. Lahti, K. Pussi, R. G. Egdell, X.-S. Wang, A. T. S. Wee, and W. Chen, Phys. Rev. B **83**, 235418 (2011).

[27] J. R. Osiecki and R. I. G. Uhrberg, Phys. Rev. B **87**, 075441 (2013).

[28] J. S. Lannin, J. M. Calleja, and M. Cardona, Phys. Rev. B **12**, 585 (1975).

[29] J. Zhuang, N. Gao, Z. Li, X. Xu, J. Wang, J. Zhao, S. X. Dou, and Y. Du, ACS Nano **11**, 3553 (2017).

[30] S. A. de Vries, W. J. Huisman, P. Goedtkindt, M. J. Zwanenburg, S. L. Bennett, I. K. Robinson, and E. Vlieg, Surf. Sci. **414**, 159 (1998).

[31] I. Meunier, J. M. Gay, L. Lapenah, B. Aufray, H. Oughaddou, E. Landemark, G. Falkenberg, L. Lottermoser, and R. L. Johnson, Surf. Sci. **422**, 42 (1999).

[32] B. Aufray, H. Giordano, and D. N. Seidman, Surf. Sci. **447**, 180 (2000).